AGU100 ADVANCING EARTH AND SPACE SCIENCE

JGR

Journal of Geophysical Research: Atmospheres

RESEARCH ARTICLE
10.1029/2018JD028951

Key Points:
- Schumann resonance is the electromagnetic phenomenon in the Earth-ionosphere cavity
- The day and night ionosphere have different properties, so that cavity is nonuniform
- The nonuniformity modifies the radio waves arriving from the global thunderstorms and thus alter the detected source bearing

Correspondence to:
A. P. Nickolaenko,
sasha@ire.kharkov.ua

Citation:
Nickolaenko, A. P., Galuk, Y. P., & Hayakawa, M. (2018). Source bearing of Extremely Low Frequency (ELF) waves in the Earth-ionosphere cavity with day-night nonuniformity. *Journal of Geophysical Research: Atmospheres*, *123*, 10,895–10,910. https://doi.org/10.1029/2018JD028951

Received 4 MAY 2018
Accepted 18 SEP 2018
Accepted article online 21 SEP 2018
Published online 8 OCT 2018

Author Contributions:
Investigation: M. Hayakawa
Methodology: M. Hayakawa
Supervision: M. Hayakawa
Validation: M. Hayakawa
Writing - original draft: M. Hayakawa
Writing – review & editing: M. Hayakawa

Source Bearing of Extremely Low Frequency (ELF) Waves in the Earth-Ionosphere Cavity With Day-Night Nonuniformity

A. P. Nickolaenko[1], Yu P. Galuk[2], and M. Hayakawa[3]

[1]A.Ya. Usikov Institute for Radio-Physics and Electronics, National Academy of Sciences of the Ukraine, Kharkov, Ukraine, [2]Mathematical-Mechanical Department, Saint-Petersburg State University, Saint-Petersburg, Russia, [3]Hayakawa Institute of Seismo Electromagnetics Co. Ltd.(Hi-SEM), The University of Electro-Communications (UEC) Alliance Center #521, and Advanced & Wireless and Communications Research Center, UEC, Chofu, Tokyo, Japan

Abstract Impact is modeled of the day-night nonuniformity of the Earth-ionosphere cavity on the source bearing. The smooth day-night interface is considered. The source is located at the 22.5° N; 0° E point, and the observer is positioned at 22.5° S; 0° E. Propagation path position corresponds to 4 hr UT (the night side) and to 8 hr UT (the dayside of morning terminator). We apply the full wave solution to determine the propagation parameters of extremely low frequency radio waves and solve the problem by using the 2-D telegraph equations. The following results were obtained: Terminator impact is absent when the propagation path is at the center of night or day hemisphere. Deviation of source bearing varies with frequency similarly to Schumann resonance pattern and may reach 3–4° at certain frequencies. A weak elliptic polarization is observed for the monochromatic radiation; its sign changes when propagation path shifts from one side of the day-night interface to the other. Temporal variations of the pulsed orthogonal components of horizontal magnetic field form a hodograph outlining complex loops, which obstructs the source bearing. Waveforms change noticeably due to frequency response of a receiver, but the maximum instantaneous deviations do not exceed 1–2°. Effect of the day-night nonuniformity on the Schumann resonance fields does not exceed the level of natural fluctuations caused by the background lightning activity. Therefore, deviations in the source bearing caused by the day-night nonuniformity might be detected exclusively for exceptionally great extremely low frequency transients.

1. Introduction

Global thunderstorms are the major source of natural radio emission in the extremely low frequency (ELF = 3–3,000 Hz) band where the global electromagnetic (Schumann) resonance is observed. It is possible to determine the current location of global thunderstorms and investigate their dynamics during the day by measuring the arrival angles of radio waves at an observatory. The source bearings are especially necessary in locating extremely powerful lightning strokes exceeding the current ELF continuous background radio signal arriving from the global thunderstorms by a factor of 10. Such huge pulses arrive at a rate of approximately once in 10 min. These powerful lightning strokes are able to modify the air conductivity in the middle atmosphere and cause the phenomena regarded as *red sprites* and *blue jets*. Therefore, it is interesting to study the spatial distribution of such strokes from a remote observatory. Since the source-receiver distances may reach many thousands of kilometers, it is desirable to determine the source azimuth as accurately as possible. The concerns are quite natural that the day-night nonuniformity of the Earth-ionosphere cavity might cause systematic errors in the source bearing. The recent paper by Mlynarczyk et al. (2017) discussed the observed deviations in the source azimuth at low frequencies. The source azimuth errors were determined from simultaneous measurements of the low-frequency radio waves and registrations of the local lightning location network. The average deviations of the source azimuths reaching 6° were recorded when the ionospheric day-night interface passes over the propagation path. We were interested in these results and estimated possible deviations in the source azimuth by using model calculations of Schumann resonance radio signals.

Computations were performed in the cavity with a smooth day-night transition (Galuk et al., 2018). The model we use is presented in Figure 1. The upper frame here depicts the height dependence of atmospheric conductivity in ambient day (curve with closed circles) and night (curve with stars) conditions. The ordinate depicts the altitude above the ground level in kilometer, and the abscissa shows the logarithm of air conductivity measures in seimen per meter. The diagram in the lower part of Figure 1 illustrates the geometry of smooth day-night interface.

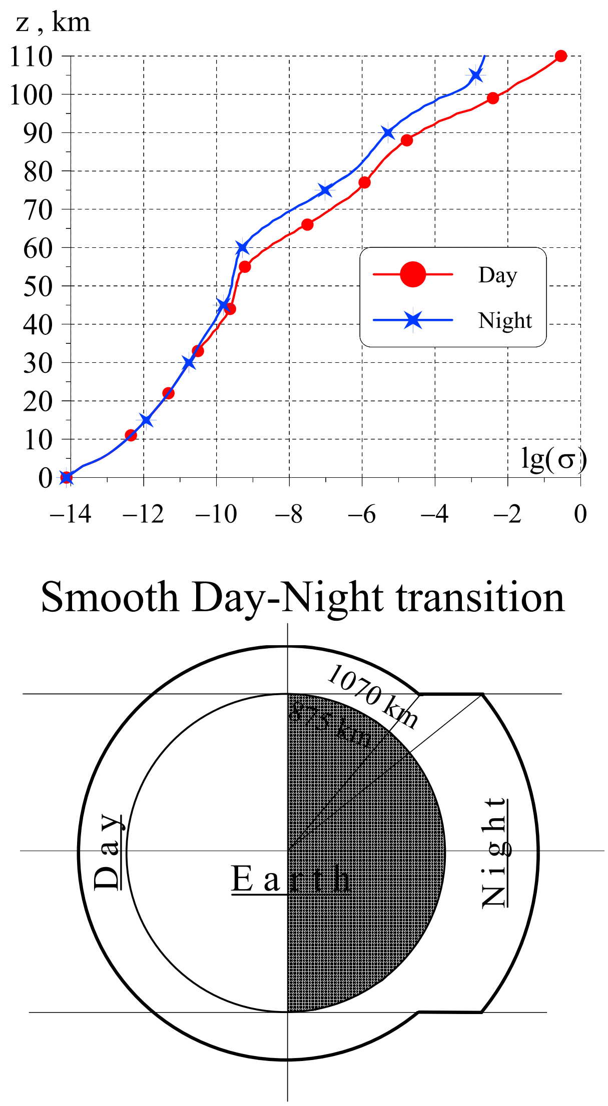

Figure 1. Earth-ionosphere cavity model used in the computations.

We postulate that properties of the middle atmosphere of the day and the night hemispheres are independent of the angular coordinates and vary only with altitude. The exception is the transition region from the light to shadow area (the solar terminator). We use a realistic model of smooth interface connecting a larger sunlit and a smaller shadow ionosphere (we do not account for the finite dimension of solar disk). The conductivity profile of ambient day is valid on the dayside and up to the distance of 875 km from the solar terminator line toward the night side. This inequality arises from the location of ionosphere in the shadow thrown by the planet and the lower boundary positioned at a definite height. The strip of 875 km is obtained for the particular height of the dayside ionosphere of 55 km, as seen in the lower diagram of Figure 1. The height of ionosphere lower boundary grows up to approximately 90 km on the night side of the globe, which corresponds to a *dawn-dusk* area lying above the dark side of the planet at distances from 875 to 1,070 km from the solar terminator line. In this 875–1,070-km interval, the parameters of ionospheric plasma vary, and we use in the model the smooth linear transition from the day characteristic heights to the night ones. One may say that horizontal changes of conductivity occur linearly from the daytime to the nighttime values.

The computations were made for the equinox period. This means that centers of the day and the night hemispheres are located at the equator, and the light-shadow boundary on the ground is coincident with the meridian. The source and the receiver occupy the same zero geographic meridian, the source latitude is equal to 22.5° N, and that of the observer is 22.5° S. Thus, the propagation path has the length of 5 Mm, and it is oriented from North to South, and it remains "parallel" to the solar terminator line during the day, as distances from the source and observer to the day-night interface are always equal to each other. Owing to such a choice, the center of the propagation path is coincident with the center of the night hemisphere on the UT midnight, and it is coincident with the center of the day hemisphere on Greenwich noon.

The propagation parameters of the ELF radio waves were computed for the given day and night profiles of the middle atmosphere conductivity by using the full wave solution in the cavity with the smooth day-night interface. The Riccati equation was used in computations (Galuk et al., 2015, 2018; Kudintseva et al., 2016; Nickolaenko et al., 2016a, 2016b, 2017). The wave fields were found by solving the 2-D telegraph equation (2DTE). In contrast to the published papers treating only the vertical electric field component, we computed also the two orthogonal components of the horizontal magnetic field in the nonuniform cavity.

We demonstrate the geometry of the problem in Figure 2. The side view of the globe is shown in the upper frame of this figure. Here the equator is drawn together with the northern 22.5° N and the southern 22.5 ° S tropic parallels: the latitude occupied by the field source and the observer. A meridian of solar terminator is also shown, and the night hemisphere is located closer to the viewer. The intersection of equator and the terminator line corresponds to 6 hr UT. We show the vertical source-observer arcs at equal distances from the terminator to the left and to the right from it. Their positions correspond to 4 and 8 hr UT (60° and 120° E longitude). The same two positions of the source-receiver path are also depicted in the lower panel of Figure 2 where the top view is used.

We use the paths parallel to the terminator line in the sense that the distances from the terminator are equal to both the source and the receiver. Such an arrangement corresponds to the ultimate deviations in the source bearing.

Indeed, let us imagine the equatorial positioning of the field source and the observer prior to treating our problem. Such a propagation path is permanently perpendicular to the solar terminator line, and the impact of

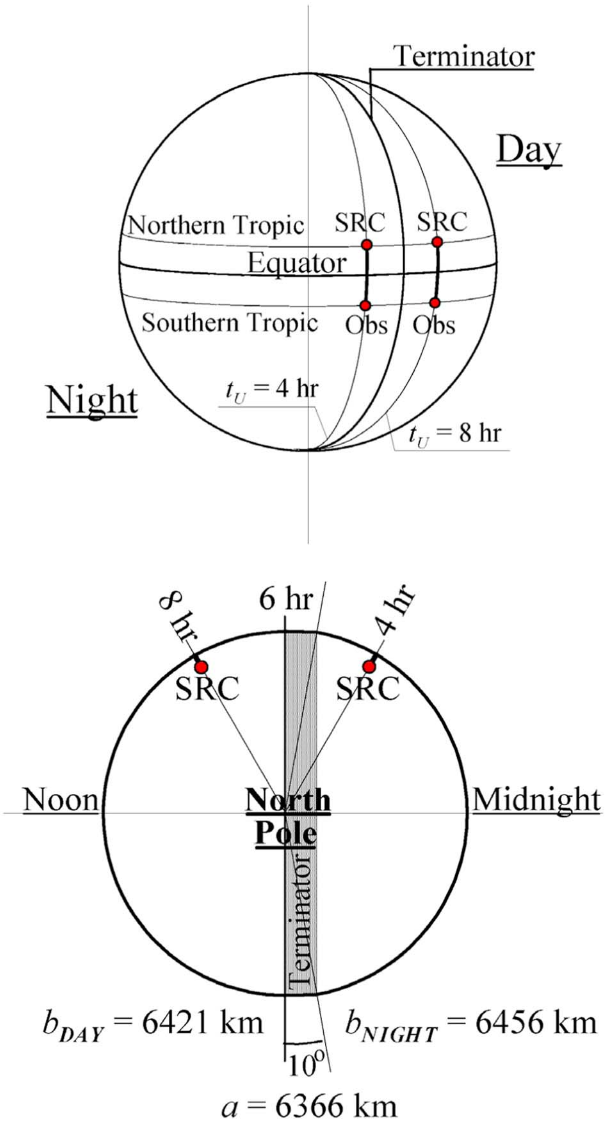

Figure 2. Positions of propagation path in the Earth-ionosphere cavity with the smooth day-night nonuniversity. SRC = source.

the day-night nonuniformity is completely absent in the source bearing. Indeed, the wave front propagating from the source might be found in any hemisphere, and its outline may vary correspondingly when crossing the day-night interface due to alterations of the propagation constant. However, the front itself remains symmetrical relative to the equator. Therefore, the normal to the wave front (which actually is the source bearing) will retain its orientation. Depending on the time of day, the radio signal amplitude might vary at the perpendicular propagation path (Galuk et al., 2018), although the propagation direction remains stable owing to the normal wave incidence on the day-night nonuniformity.

The situation is completely different at the parallel paths, especially, when the source and the observer come into the vicinity of solar terminator. In this case, the night and the day sides of the wave front have unequal phase velocities, and this will cause the ultimate excursions of the wave front normal.

Validity of above speculations is obvious for a sharp day-night interface, whereas we apply a more realistic smooth night-day transition of 1,070 km width (see Figure 1). Because of the finite width of the day-night interface, we must place the propagation paths at definite distance outside the terminator area. Two characteristic times were chosen $t_U = 4$ and $t_U = 8$ hr corresponding to ±30° angular distance between the solar terminator and the propagation paths. The structure of the smooth day-night interface in the ionosphere was explained by the lower diagram of Figure 1. Since the spherical Earth has the 40-Mm circumference, its radius is $a = 6{,}366$ km. By assuming that the lower boundary of the daytime ionosphere lies at 55-km altitude above the ground, we obtain its radius $b_{\mathrm{DAY}} = 6{,}421$ km. The night ionosphere has the height of 90 km, so its radius is $b_{\mathrm{NIGHT}} = 6{,}456$ km. By using these values, one will obtain the distances of 875 and 1,070 km shown in Figure 1. The above radii clearly indicate that a descriptive lower diagram of Figure 1 cannot show the actual proportions.

We try to show the situation in a more realistic way in Figure 2 (the bottom panel). It schematically shows the upper view of the ionosphere boundary from the North Pole side. The daytime ionosphere is found on the left, and the night ionosphere is on the right. The dark strip to the right from the solar terminator depicts the area of smooth transition of ionosphere parameters from their day to the night quantities. The angular width of this area is ~10° (1,070 km along the ground surface). The centers of the night and the day hemispheres are visible together with the morning terminator $t_U = 6$ hr. The rays to the sides from the terminator line have the tilt of ±30°, and they mark positions of $t_U = 4$ hr and $t_U = 8$ hr meridians. The thick bars at these meridians denote the propagation paths visible from above the North Pole. Only the source points are visible marked by the circles labeled SRC (source). A second half of propagation path and the observer are hidden behind the horizon (the equator line).

2. Source Bearing

The main problem associated with applications of 2DTE proposed by Madden and Thompson (1965) for computing the ELF radio wave propagation was the absence of description in what a way the elementary inductance L, capacitance C, and resistance R might be obtained for the two-dimensional RLC network modeling the Earth-ionosphere cavity, as well as the source parameters (right-hand side of the equation). The paper did not either describe how to convert the 2DTE solution into the electromagnetic field components. Probably therefore, application of 2DTE in Schumann resonance studies was delayed. A rigorous justification was given by Kirillov (1996, 1998), Kirillov et al. (1997), and Kirillov and Kopeykin (2002, 2003) for the applicability of the 2DTE itself and for parameters involved in equations. This approach was applied in studies by Pechony and Price (2004) and Pechony (2007). An independent approach to 2DTE implications at ELF was suggested by Kulak et al. (2003).

According to Kirillov's formulation, the 2DTE have the following differential form:

$$\operatorname{div}\left(\frac{\operatorname{grad}u}{H_L}\right)+k^2\frac{u+u_s}{H_C}=0, \tag{1}$$

where k is the wave number; u is the sought voltage; u_S is the voltage of the external sources of the field.

Parameters involved in equation (1) are the complex quantities associated with the elementary inductance L and the capacitance C—the so-called "electric" H_C and the "magnetic" H_L heights. These parameters have a clear physical meaning: the real part of H_C is the height of the electric field penetration into the ionospheric plasma for the normal incidence of the plane wave on the air-plasma interface. The real part of H_L is the altitude of the magnetic field penetration into the nonuniform ionospheric plasma. The imaginary parts of these parameters are associated with the energy loss; they are proportional to the height scales of the conductivity profile in the middle atmosphere. For example, one obtains $H_C = h$ in the model of a sharply bounded ionosphere, uniform along the height with a constant conductivity σ starting from the altitude h. The magnetic height H_L exceeds the electric height H_C by the complex skin depth of the ionosphere, that is, $H_L = h + \sqrt{\frac{\mu_0}{i\omega\sigma}}$.

The propagation constant ν and the normalizing integral N_0 are used in solving the ELF radio propagation problem, and these are derived by using the full wave approach (Galuk et al., 2015; Hynninen & Galuk, 1972; Nickolaenko et al., 2016a, 2016b, 2017) in the regular Earth-ionosphere cavity. Fortunately, there are formulas linking these parameters with quantities used in 2DTE: the complex heights H_C and H_L. First of all, it turns out that parameters N_0 and H_C might be set equal to each other $H_C = N_0$ within the ELF band. This equality is a nontrivial one indeed, since the quantities are found from completely different considerations. Moreover, the electric altitude H_C is introduced as a linear form relevant to the vertical electric field component (E):

$$H_C(\theta,\varphi)=\frac{\int_a^\infty E(r,\theta,\varphi)dr}{E(a,\theta,\varphi)}, \tag{2}$$

while the normalizing integral $H_c(\theta,\varphi)=E_r^{-1}(a,\theta,\varphi)\int_a^\infty E_r(r,\theta,\varphi)dr$ N_0 is defined as a quadratic form of the eigen-function $\rho_0(r, \theta, \varphi)$ (Kirillov, 1996; Kirillov et al., 1997; Kirillov & Kopeykin, 2002, 2003):

$$N_0=\left[\frac{a}{\rho_0(a)}\right]^2\int_a^\infty\frac{\rho_0^2(r)}{r^2}dr=-a^2ik\frac{\partial}{\partial\lambda}\delta(a,\lambda). \tag{3}$$

Here a is the Earth's radius, and $\rho_0(r, \theta, \varphi)$ is the eigen-function of spherical Earth-ionosphere cavity.

Second, the following dispersion relation is valid: $(kaS)^2=\nu(\nu+1)=\frac{H_L}{H_C}$ where S is the complex sine of the incidence angle of a plane wave on the ionosphere, and $\nu(f)$ is the ELF complex propagation constant.

Thus, the algorithm of finding parameters involved in the 2DTE is reduced to the following. First, parameters ν and N_0 are computed by using the procedure described by Hynninen and Galuk (1972), Galuk et al. (2015), and Nickolaenko et al. (2016a, 2016b, 2017). The system of two differential equations is solved numerically for the function δ (ionospheric surface impedance) and its derivative with the parameter $\lambda = \nu(\nu + 1)$ being the separation constant of the wave equation in the spherical coordinate system. The propagation constant ν is found by Newton iterative procedure with the initial value of $\nu = ka$. The normalizing integral N_0 is expressed in terms of the impedance derivative with respect to the parameter λ.

Further, one obtains the 2DTE parameters in the entire range of variables θ and φ by using the above relations $H_C = N_0$ and $H_L = H_C{\cdot}\nu{\cdot}(\nu + 1)$. The 2DTE (1) acquires the following form in the spherical coordinate system $\{r, \theta, \varphi\}$:

$$\frac{H_L(\theta,\varphi)}{\sin\theta}\frac{\partial}{\partial\theta}\left(\frac{\sin\theta}{H_L|\theta,\varphi|}\frac{\partial u}{\partial\theta}\right)+\frac{H_L(\theta,\varphi)}{\sin^2\theta}\frac{\partial}{\partial\varphi}\left(\frac{1}{H_L(\theta,\varphi)}\frac{\partial u}{\partial\theta}\right)+(kaS)^2(u+u_s)=0, \tag{4}$$

where the external source u_S (the vertical electric dipole source of the P_0 moment) is found from the formula $u_S = P_0\frac{\delta(\theta)}{2\pi\varepsilon_0 a^2\sin\theta}$.

In distinction from works by Kirillov group, equation (4) is solved by the grid method using the so-called *block tri-diagonal matrix algorithm* regarded in Russian literature as *matrix sweep technique* (Samarskyj, 2001). An advantage of this approach is that the solution is constructed at the entire surface of the globe.

After obtaining the solution of 2DTE in a form of $u(\theta, \varphi)$, which is the voltage between the ground surface and the ionosphere, it is possible to turn to physically measurable variables: the vertical electric field component E_r and the horizontal magnetic field components H_θ and H_φ:

$$E_r=\frac{u(\theta,\varphi)}{H_C}, \tag{5}$$

$$H_\varphi=\frac{i}{kaZ_0H_L}\frac{\partial u}{\partial\theta}, \tag{6}$$

$$H_\theta=\frac{i}{kaZ_0H_L\sin\theta}\frac{\partial u}{\partial\varphi}. \tag{7}$$

All the fields in equations (5)–(7) are complex functions of frequency since they are the Fourier transforms of the real functions of time. Z_0 is the free space wave impedance. Only the E_r component was addressed in all publications using 2DTE. Since the goal of our study is an impact of the day-night nonuniformity on the source bearing, we have to additionally compute the orthogonal magnetic field components H_θ and H_φ.

The vertical electric and two mutually orthogonal horizontal magnetic field components are recorded in experimental observations. The latter are usually directed from west to east ($H_{WE} = H_\varphi$) and from south to north ($H_{SN} = -H_\theta$) in the geographical coordinate system. When the orientation of the magnetic antennas is changed (by rotating them by an angle α around the vertical *OZ*- axis), the new field components $H_{X'}$ and $H_{Y'}$ are expressed in terms of the old components $H_X = H_{WE} = H_\varphi$ and $H_Y = H_{SN} = -H_\theta$ by using the following matrix $\begin{pmatrix}H_{X'}\\H_{Y'}\end{pmatrix}=\begin{pmatrix}\cos\alpha & \sin\alpha\\-\sin\alpha & \cos\alpha\end{pmatrix}\begin{pmatrix}H_X\\H_Y\end{pmatrix}$. We assume in what follows that magnetic antennas are oriented along the cardinal directions, so that the angle $\alpha = 0$.

We solve in what follows the source-bearing problem from a particular observation site. Direction to the source is coincident with the geodetic line connecting the transmitter and the receiver. Direction toward the source is regarded as perpendicular to the horizontal magnetic field vector at the observatory; therefore, in the regular (uniform) cavity, the longitudinal field component H_θ is equal to zero. This field is generally nonzero in a nonuniform cavity, and the source bearing deviates from the actual meridional direction. It should be noted also that, because of the phase mismatch between the H_θ and H_φ components at a given frequency, the tip of the total horizontal magnetic field vector moves along an ellipse in time, the trajectory is regarded as the polarization ellipse. The tilt angle ψ of the semimajor axis of this ellipse relative to the direction perpendicular to the geodetic line (direction to the source) is the sought azimuth of the source. It is calculated from the formula:

$$\psi=-\frac{1}{2}\tan^{-1}\left(\frac{2\left[\mathrm{Re}(H_\phi)\,\mathrm{Re}(H_\theta)+\mathrm{Im}(H_\phi)\,\mathrm{Im}(H_\theta)\right]}{|H_\phi|^2-|H_\theta|^2}\right) \tag{8}$$

When one of the field components (usually the H_θ component) is much smaller than the other one, one can use the simpler formula: $\psi \cong -\,\mathrm{Re}\left(\frac{H_\theta}{H_\phi}\right)$.

3. Model Results in the Frequency Domain

It was shown by Galuk et al. (2018) that impact of the day-night interface arises due to reflections of ELF radio waves incident from the field source on the ionosphere irregularity in the Earth-ionosphere cavity. The

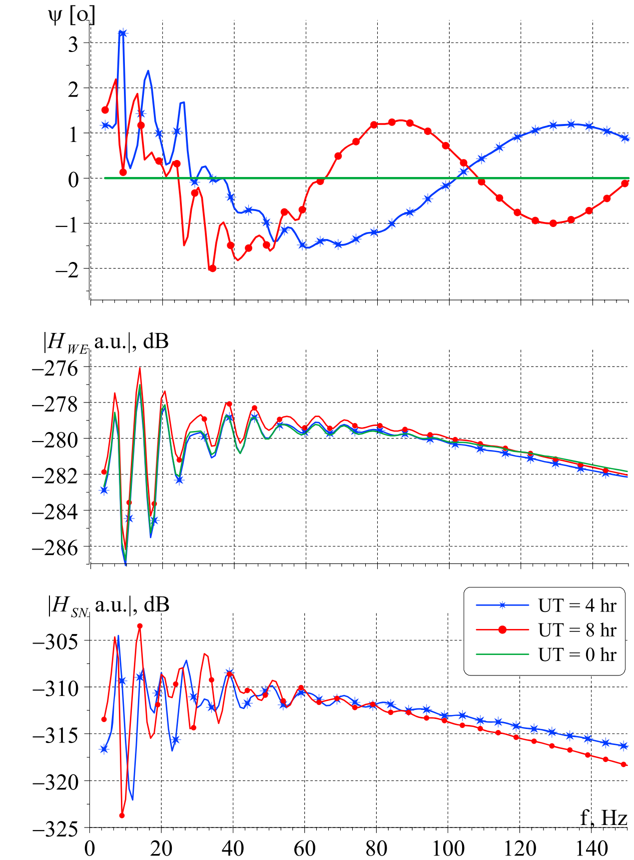

Figure 3. Spectra of the source bearing and magnetic field components. The upper panel shows the source azimuth as a function of frequency for three positions of propagation path relative to the day-night nonuniformity. Two lower panels depict the amplitude spectra of the H_{WE} and H_{SN} field components that govern the source azimuth deviations.

reflection characteristics depend on the position of propagation path against the nonuniformity. Obviously, the geometry of the problem becomes symmetric at UT noon and the UT midnight in spite of the day-night nonuniformity. At these time moments, the amplitude of wave reflected from the terminator turns into zero at the observation site, and the effect of the inhomogeneity disappears. Reflections increase when the propagation path comes closer to the morning or evening edge of the day or the night hemisphere. We performed computations on the UT times $t_U = 4$ and $t_U = 8$ hr for the smooth day-night transition model having the dawn-dusk zone extended to 1,070 km from the solar terminator line (see Figure 1). Owing to daily rotation of the Earth, the source and the receiver occupy the 60° E meridian when $t_U = 4$ hr (the night side in the vicinity of the morning terminator). When $t_U = 8$ hr, the propagation path moves to the 120° E longitude (the day side of morning terminator).

The upper panel in Figure 3 shows the frequency dependence of the source bearing, and we suggest that the field is produced by the vertical electric dipole source with the current moment independent of frequency. This means that the charge moment of source varies in time as the step function (similarly to a cloud charge moment), and the current moment is a Dirak's delta function (similarly to that of an ideal lightning stroke). The abscissa in all three frames of Figure 3 depicts the frequency in the band 4–150 Hz, and the ordinate shows the source azimuth in degrees derived from the ratio of $H_{SN}(t)$ and $H_{WE}(t)$ field components. We count the source bearing measured at the observation point as in a compass: the positive values are found to the east (clockwise) from the North direction, and the negative azimuths are to the west from the North direction (counterclockwise). We must also have in mind that the "unusual" H_{SN} field component is equal to zero when $t_U = 0$ and $t_U = 12$ hr. This particular field component arises from the wave reflections from the day-night interface, and owing to the symmetry of the problem, the source bearing points strictly to the north at these particular time moments.

The upper frame in Figure 3 depicts frequency variations of the source bearing. The green straight line corresponds to the propagation path symmetrically positioned at the center of the night hemisphere ($t_U = 0$ hr) when no deviations arise in the source azimuth. The blue curve with stars corresponds to the path location on the shaded side of the planet ($t_U = 4$ hr), and the red curve with the closed circles shows the data on the day-side of morning terminator ($t_U = 8$ hr). One may observe that deviations from the actual direction toward the source depend on the signal frequency, and they may slightly exceed 3°. The average source bearing is shifted eastward, toward the center of the day hemisphere on the dayside of the planet ($t_U = 8$ hr). On the night side of the morning terminator ($t_U = 4$ hr), the source bearing is shifted, on average, westward from the actual direction (toward the center of the night hemisphere).

Such behavior of the source bearing is conditioned by two factors. The first of them is amplification of wave reflections when propagation path approaches the day-night interface: the reflections are amplified at gliding incidence angles at the ionospheric nonuniformity. This is why we observe no deviations when $t_U = 0$ hr, while data for $t_U = 4$ and $t_U = 8$ hr show variations in the source bearing. Excursions of the source azimuth demonstrate obvious marks of Schumann resonance up to ~80-Hz frequency. The second factor, which becomes especially obvious at higher frequencies, is the wave reflection from the day-night interface. One may conclude that the reflection coefficient of ELF radio wave from the terminator changes its sign when propagation path is shifted from the night side to the dayside of interface. Therefore, at higher frequencies, the observed source bearings deviate in the opposite directions from its actual zero value.

Two lower panels in Figure 3 show amplitude spectra of horizontal magnetic field components H_{WE} (f) and H_{SN} (f). The ordinates depict the spectral amplitude of the "regular" and the "anomalous" field component both measured in decibel relative arbitrary units. The field component H_{SN} is much smaller than H_{WE}: this

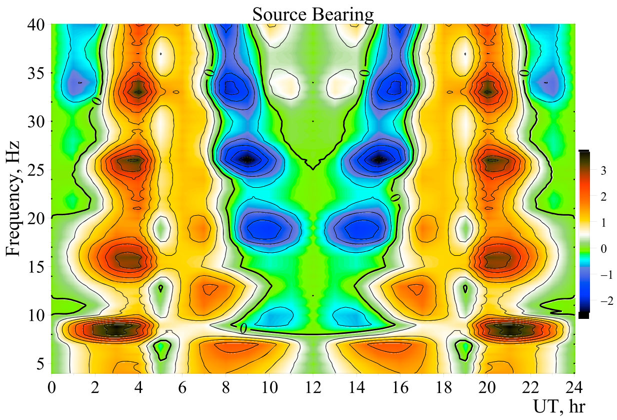

Figure 4. Source bearing of the nonuniform Earth-ionosphere cavity over the time-frequency plane.

is the field arising from the wave scattering by the nonuniformity. The blue curve with the stars corresponds to the propagation path located at the terminator night side ($t_U = 4$ hr), and the red curve with closed circles corresponds to $t_U = 8$ hr. The "reference" green spectrum of the "midnight" $t_U = 0$ hr field $|H_{WE}(f)|$ is very close to the both *near terminator spectra*. All regular field components $H_{WE}(f)$ demonstrate the customary Schumann resonance pattern pertinent to the source-observer distance of 5 Mm, although minute deviations exist relevant to the position of propagation path relative to terminator. The small scattered field component $H_{SN}(f)$ also has maxima at Schumann resonance frequencies. But its general outline is different, as it depends on the reflections from the day-night interface. Existence of two nonzero horizontal magnetic field components causes perturbations in the source bearing depending on signal frequency, and these deviations carry the Schumann resonance pattern. The plots in the lower panels explain how deviations arise in the source bearing.

The noted properties of reflected waves might be derived from the following qualitative straightforward considerations. A fictitious field source should be introduced in addition to the actual one in the presence of a reflecting boundary. It is located on the other side of the day-night interface symmetrically to the actual source. The fields from the true and fictitious sources are summed at the observation point, and the horizontal magnetic field vector is perpendicular to the line connecting the observer and the true source in the first case, and it is orthogonal to the line connecting the observer and the fictitious source in the second case. The horizontal magnetic field of the direct wave arriving from the true source is always oriented along the φ axis or along the west-east direction in the chosen geometry of the problem. The magnetic field of the wave reflected from the terminator (the wave coming from the source image) is tilted and has two projections $H_\varphi = H_{WE}$ and $H_\theta = H_{SN}$ at the observatory. The resulting amplitude of the west-east component deviates from the field amplitude in the uniform cavity. In addition, an anomalous south-north component appears, which alters the observed source bearing. It is obvious that perturbations of the source azimuth depend on the geometry of the problem, in particular, on the path distance from the day-night interface.

The above considerations become rigorous when the problem is of Cartesian flat geometry, the terminator is sharp, and the reflections from interface are perfect. These conditions are not held in our model. Therefore, the explanation suggested remains qualitative and might be used only for interpretation of computational results.

Frequency variations of source bearing reminding of Schumann resonance pattern were presented in experimental observations by Belyaev et al. (1999). However, the nature of those much greater deviations was different; they apparently originated from the particular excitation conditions of the cavity during measurements when both the African and the South American thunderstorm centers were active simultaneously, while the directions toward these centers departed by approximately 90° from the observation site (Belyaev et al., 1999).

Figure 2 shows frequency variations of the source bearing for discrete time moments. A much more comprehensive picture of deviations is obtained when plotting the source azimuth in the form of a 2-D map over the time-frequency plane as seen in Figure 4.

The universal time is shown along the abscissa in Figure 4 ranging from 0 to 12 hr. The ordinate shows the frequency from 4 to 40 Hz, and the source azimuth measured at the observation site is shown by color inking. The color scale is shown to the right of the map. The center of propagation path is coincident with the center of the night or day hemisphere, when $t_U = 0$ and $t_U = 12$ hr correspondingly. Figure 4 demonstrates that deviations in the source bearing are equal to zero $\psi = 0$ at these time moments. The source azimuth map is symmetric against the vertical axis $t_U = 12$ hr, that is, the distribution of the $0 < t_U < 12$ hr interval might be reflected about this axis, and thus, we obtain distribution in the interval $12 < t_U < 24$ hr. As might be seen in Figure 4, deviations in the source azimuth depend substantially on the frequency and the position of propagation path relative to the terminator line. The maximum deviations may slightly exceed ±3°.

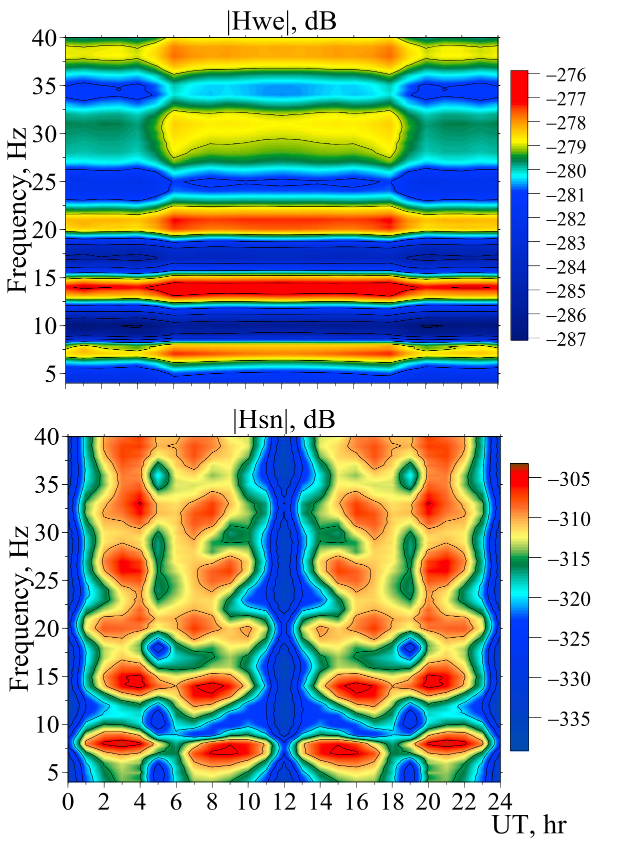

Figure 5. Amplitude of magnetic field horizontal components above the time-frequency plane. The regular H_{WE} component is shown in the top panel; the "anomalous" H_{SN} component in the bottom panel.

In a uniform Earth-ionosphere cavity, the observed horizontal magnetic field has only the single component $H_\varphi = H_{WE}$ oriented along the geographic parallel, provided that the source and observer occupy the same meridian. In the presence of nonuniformity of the day-night type, the amplitude of this component slightly changes, and an additional field component $H_\theta = H_{SN}$ appears of small amplitude. It is directed along the meridian, and the source bearing is distorted as a result. Figure 5 shows amplitude distributions of the H_{WE} and H_{SN} fields over the time-frequency coordinate plane. These amplitudes are measured in relative units, and the decibel scale is used.

The upper panel in Figure 5 shows the amplitude of H_{WE} (t_U, f) component. Here the stripes of resonance maxima and minima in the field amplitude are clearly visible. One may observe that the amplitude of the horizontal magnetic field increases in the time interval $5 < t_U < 6$ hr when the propagation path is found under the dayside of ionosphere. Such behavior of the field amplitude is familiar, since it is caused by the change in the ionosphere height (see, e.g., Galuk et al., 2018).

The lower panel in Figure 5 shows the amplitude of the "scattered" H_{SN} (t_U, f) field. The pattern in this figure is much more complicated. Here one meets a succession of maxima and minima of the amplitude, which arose due to reflections from the day-night nonuniformity. The interference maxima and minima become especially pronounced at resonance frequencies of 8, 14, 26, and 32 Hz. The number of maxima increases with growing frequency, that is, the peaks are visible along the horizontal lines of fixed frequency. Such behavior is readily explained by the decrease of the radio wavelength.

A remarkable feature is clearly visible in the lower frame of Figure 5 pertinent to reflections from the day-night interface: concentration of maxima (red spots connected by yellow strips) and minima (blue spots inside the green strips) of the H_{SN} (t_U, f) field is extended along the system of hyperbolas. It is easy to guess that such a *phase difference* structure arises from the interference of the direct wave and the wave reflected from terminator due to their nonzero path difference. Thus, two processes are involved in formation of spatial amplitude distribution of the anomalous H_{SN} field. From one hand, this is the Schumann resonance that forces the increase of spectral density at frequencies of 8, 14, 20 Hz, and so forth. On the other hand, the wave reflected from the terminator imposes additional amplitude modulation on the resonance structure. Relevant reflections from terminator and their properties were described in the paper by Galuk et al. (2018) for in the vertical electric field component. Now, we observe that the ELF wave bouncing becomes even more pronounced, as it arises in the form of anomalous longitudinal H_{SN} horizontal magnetic field component.

4. Source Bearing in the Time Domain

We worked in the frequency domain until now and considered the field spectra. This allowed for estimating the expected distortions in the source bearing caused by the ionospheric day-night nonuniformity. In the experiment, the source bearing is usually deduced from the time realizations of two mutually orthogonal components of the magnetic field H_{WE} and H_{SN}. To model actual measurements, we apply the Fourier transform toward the complex spectra of the fields $H_{WE}(f)$ and $H_{SN}(f)$ and obtain their temporal conjugates $H_{WE}(t)$ and $H_{SN}(t)$. First of all, we consider the simplest case of a monochromatic ELF radio wave.

Consider the vertical electric dipole source emitting a monochromatic radio wave at the frequency of 8 Hz. After computing the spectral components of the fields, we perform the Fourier transforms and obtain the time domain realizations corresponding to the particular positions of propagation path relative to the nonuniformity. Figure 5 presents the computations time domain results for two moments of universal time

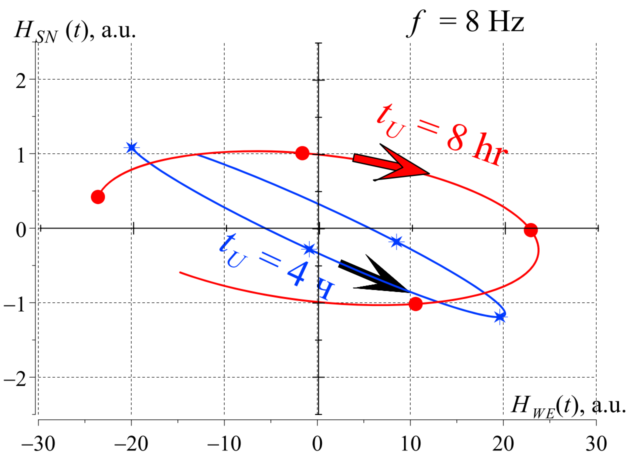

Figure 6. Hodographs of monochromatic horizontal magnetic field vector at 8-Hz frequency for $t_U = 4$ and $t_U = 8$ hr.

$t_U = 4$ and $t_U = 8$ hr, when the propagation paths are found near the day-night interface under the shadow and the illuminated side of ionosphere, respectively.

The hodographs (or Lissajous figures) are shown in Figure 6 calculated for the horizontal magnetic field vector. The horizontal axis depicts temporal changes of the field component $H_{WE}(t)$ in arbitrary units, and the vertical axis shows the $H_{SN}(t)$ field component measured in the same units. The time t acts as a parameter. Since the field amplitudes are departed by almost two orders of magnitude, the scales of abscissa and the ordinate also deviate by the factor of 10. One can observe in Figure 6 that a monochromatic 8-Hz wave in the nonuniform Earth-ionosphere cavity acquires an elliptical polarization, and this is quite unexpected for a resonator formed by the ground and isotropic ionosphere plasma. The ellipticity coefficient is rather small, and it depends on the time of day. This means that rotation direction of the horizontal magnetic field vector changes to the opposite one when the propagation path crosses the terminator line. The right elliptic polarization is observed when $t_U = 4$ hr, and the left one is observed when $t_U = 8$ hr. The elliptical polarization appears owing to a small phase delay between the reflected field $H_{SN}(t)$ against the regular meridional $H_{WE}(t)$ component. The delay is explained by somewhat greater length of the propagation path of the wave reflected from the terminator (observer-source image) exceeding the 5-Mm observer-actual source distance. The small absolute value of reflection coefficient from the terminator turns out to be negative when $t_U = 4$ hr when the wave is incident at the nonuniformity from the night side, and it turns out to be positive when $t_U = 8$ hr when the wave is incident at the nonuniformity from the dayside (cf. with Galuk et al., 2018). However, the ellipticity coefficient in all cases is close to zero, and the field polarization only slightly deviates from the linear one.

Besides the small ellipticity, the tilt is equally insignificant of the major axis of the polarization ellipse to the *OX* axis, which is about a few degrees: this is actually the deviation in the field source azimuth. The ellipticity coefficient and the tilt angle are equal to zero in the uniform cavity, so that the tip of the horizontal magnetic field vector moves in time along the straight line perpendicular to the source-receiver great circle arc. This line is coincident with the *OX* axis in Figure 6. Obviously, the ellipticity coefficient and the tilt of polarization ellipse depend on the signal frequency, but the observed source azimuth will deviate from its actual zero value by about ±3°as Figure 3 demonstrates.

The real signals arriving at the observer in the Earth-ionosphere cavity from the lightning discharges are of the pulsed nature, and the most powerful of them is regarded as ELF transients or the Q-bursts. Pulses occupy a significant frequency range, which is determined by the band-pass width of the Earth-ionosphere cavity being about 100 Hz (Bliokh et al., 1980; Nickolaenko & Hayakawa, 2002, 2014). Simultaneously, deviations in the source azimuth from its true zero value depends on the frequency, as we observe in the spectral data presented in Figures 3 and 4.

It is not clear in advance what the resulting deviations will be in the bearing of the pulsed lightning source deduced in the time domain. In order to obtain the corresponding data, we computed the complex spectral field components in the frequency band up to 256 Hz for the same positions of propagation paths ($t_U = 4$ and $t_U = 8$ hr). Afterward, we found the pulsed waveforms of the three field components $E_r(t)$, $H_{WE}(t)$, and $H_{SN}(t)$ by using the fast Fourier transform. The magnetic fields are shown in Figure 7 together with magnetic field hodographs (Lissajous figures) of the model Q-bursts.

Figure 7 contains two panels; the left one presents the data computed for $t_U = 4$ hr, and the right one corresponds to $t_U = 8$ hr. The main graphs in each panel show the waveforms of Q-bursts. Abscissa in these plots shows the time in milliseconds passed from the beginning of the delta pulse radiated by the lightning stroke (it was assumed in computations that amplitude of the source moment is independent of frequency). Smooth curves correspond to the regular field components $H_{WE}(t)$. They correspond to the left ordinates and are marked by the inscription *direct wave*, and the fields are measured in arbitrary units. Curves with asterisks of the major graphs of Figure 7 show the temporal variations of the anomalous field component

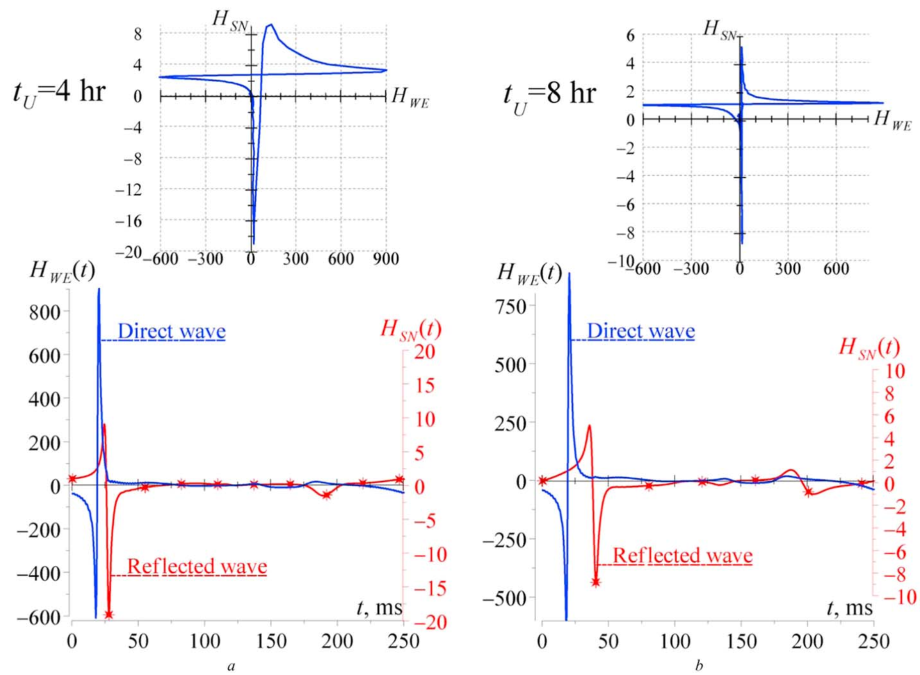

Figure 7. Waveforms and hodographs of extremely low frequency transients for the 5-mm source-observer distance. (a) Position of propagation path corresponds to 4 hr UT; (b) the propagation path location corresponds to 8 hr UT.

the field $H_{SN}(t)$, which is present only in the cavity with the day-night nonuniformity and arises due to wave reflections from the terminator. These curves are plotted against the right ordinates and are labeled "reflected wave."

The Lissajous figures are shown in the upper right corner of each panel for the pulsed signals $H_{SN}(t)$ and $H_{WE}(t)$ computed for $t_U = 4$ and 8 hr. We use the customary geographic orientation of the axes: the field component H_{WE} is plotted along the abscissa, and the field H_{SN} is shown along the ordinate. The time is the parameter. We used different scales along the axes, as the field amplitudes strongly deviate from each other.

Figure 7 indicates that computed waveforms of the pulsed ELF transients in the regular field component the field $H_{WE}(t)$ are similar to the data computed in the uniform Earth-ionosphere cavity (Nickolaenko & Hayakawa, 2002, 2014). The pulse of direct wave arrives at the observer approximately 20 ms after the lightning stroke initiation in this magnetic field component being perpendicular to the source-observer great circle arc. Another pulse of opposite polarity arrives in this component from the source antipode approximately 125 ms after the moment of discharge. It should be noted that this standard form of a Q-burst for the 5-Mm source distance is observed regardless the time of the day of the position of the propagation path relative to the terminator line. Of course, there are deviations in the $H_{WE}(t)$ curves computed for $t_U = 4$ and 8 hr, but their magnitude is very small, about 1%, which makes them practically insignificant.

The pulses in the $H_{WE}(t)$ field component originating due to wave reflections from the day-night interface are somewhat delayed behind the arrival time of direct wave. The time delay of the pulse reflected from the terminator relevant to $t_U = 4$ hr is smaller than the delay for $t_U = 8$ hr. This difference is originated from the structure of the smooth day-night transition having the shadow region at the ionospheric heights smaller than the illuminated area (see Figure 1). As a result, the distance from the propagation path to the ionospheric day-night interface is greater when $t_U = 8$ hr, and the path is found on the dayside of morning terminator. The amplitude of reflected field is noticeably smaller when $t_U = 8$ hr than that $t_U = 4$ hr. It should also be noted that the waveforms of the pulses became slightly elevated above the abscissa axis due to the particularities of fast Fourier transform computations, which is unimportant for our analysis.

Hodographs of the broadband ELF transients are demonstrated in the insets in Figures 7a and 7b. They have rather complex shape, which excludes detection of a stable deviation of the source bearing from its actual

10.1029/2018JD028951

zero value in observations of the temporal shape of the pulses. It should also be taken into account that amplitude of the reflected pulse in the component $H_{SN}(t)$ is smaller than that of the "regular pulse" in the $H_{WE}(t)$ component by a factor of approximately 50. Since registrations of Q-bursts are performed in the presence of regular continuous background noise signal from the bulk of ordinary lightning strokes and the Q-burst amplitude exceeds the root-mean-square background amplitude by a factor up to 10, the signals reflected from the nonuniformity will be hidden in this continuous background noise. This will impede confident detection of deviations in the source bearing caused by the day-night interface by using records of ELF transients even when an ideal broadband receiver with a frequency response independent of frequency is used.

5. Explicit Source Bearing

Direction toward the source is unambiguously determined only in simultaneous measurements of vertical electric and two orthogonal horizontal magnetic field components. In this case, one can construct a vector of power flux (Umov-Poynting vector). The relevant computations might be done either in the time or in the frequency domain. We confine ourselves to the time domain where the vector components are computed from the following vector product:

$$\vec{P}(t) = \vec{E}(t)\times\vec{H}(t), \tag{9}$$

$$P_\theta = P_{NS} = -E_r(t)\cdot H_\phi(t) = -E_r(t)\cdot H_{WE}(t), \tag{10}$$

$$P_\phi = P_{WE} = E_r(t)\cdot H_\theta(t) = E_r(t)\cdot H_{SN}(t). \tag{11}$$

Figure 8 shows the results of the Umov-Poynting vector computations in the time domain. The time in milliseconds from the beginning of the lightning stroke is plotted along the abscissa on both panels of the main graphs. The left panel corresponds to the propagation path position when t_U = 4 hr, and the right panel corresponds to the position when t_U = 8 hr. The smooth lines relative to the left ordinates show in the main graphs the temporal variations of the components of the vector of electromagnetic energy flux along the meridian $P_{NS}(t)$. The lines with stars in Figure 8 are plotted against the right ordinates, and they show changes of the $P_{WE}(t)$ component directed along the parallel. It might be seen that regardless of the path location relative to the nonuniformity, the major energy flux is directed along the meridian from north to south, that is, from the source to observer. The double pulse is observed in this component characterized by a narrow minimum. The waveforms of the major pulses are practically coincident in Figures 8a and 8b.

The anomalous component of the power flux $P_{WE}(t)$ is depicted by lines with asterisks, which is a bipolar pulse at the head that is followed by more complex variations. This component is much smaller in amplitude than the major power flux and significantly changes when the propagation path is moved relative to the day-night interface.

Insets in the panels of Figure 8 are located in the upper right corner, where they illustrate the hodographs (Lissajous figures) of the complete Umov-Poynting vector in the initial part of the pulse. The scale along the abscissa in the insets is greatly decreased in comparison with the scale along the ordinates. This allows us to show the details in the evolution of the power flux. One may observe that the power flux changes rather fast; it reaches twice the well-defined maxima near t = 18.1 and t = 20.5 ms for t_U = 4 hr and t = 18.6 and t = 20.5 ms for t_U = 8 hr. The outlines of temporal changes of the Umov-Poynting vector as well as the times of maximum values depend on the position of the path relative to the day-night interface. This is caused by the difference in distances passed by the waves reflected from the terminator.

The first maximum in the Umov-Poynting vector hodograph refers to the direct impulse coming from the source, and the second one is relevant to the reflections from the ionospheric nonuniformity. The figure shows that the power flow deviates from the meridian plane in opposite directions. However, these deviations are of minor practical interest, since deviations from the north-south line are rather small, and they constitute fractions of a degree. In addition, they are separated by the time interval of ~1 ms, and this is a too small value for a typical sampling frequency (200 Hz) in the data acquisition systems used in the Schumann resonance studies. Such small and rapid changes in the flux of electromagnetic power hardly will be detected in the usual Schumann resonance records.

10.1029/2018JD028951

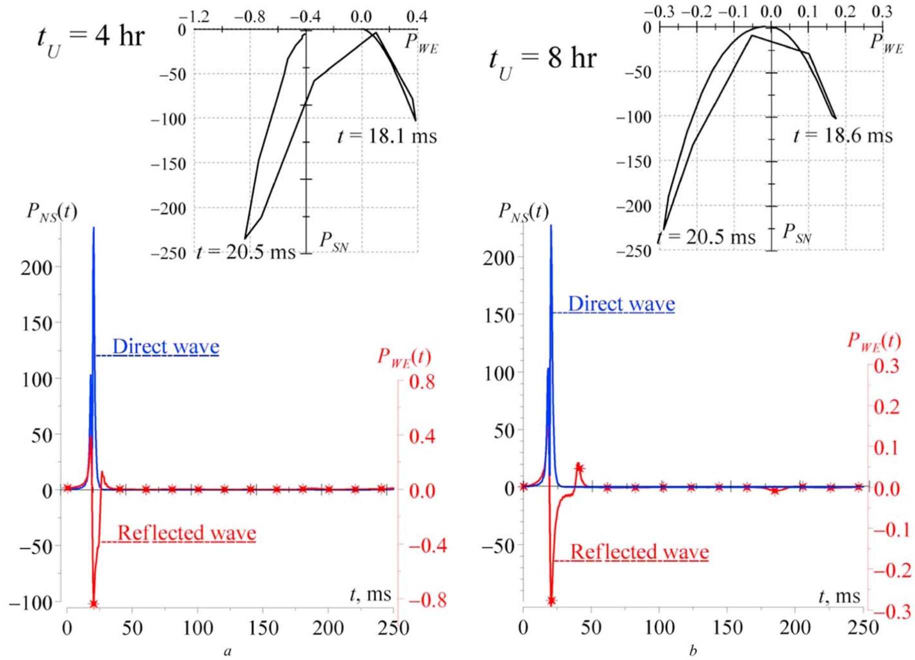

Figure 8. Waveforms and hodographs of the Umov-Poynting vector. (a) The propagation path location corresponds to 4 hr UT; (b) the location of the path corresponds to 8 hr.

6. Influence of Receiver Frequency Response

Special receivers are used in real measurements of Schumann resonance, which form a "rectangular" frequency response in the 4–40-Hz band combined with a rejection of signals at the frequency of power supplies of 50 Hz. Impact of such a typical receiver on the shape of the received pulse was addressed by Yatsevich et al. (2014). We consider the influence of a receiver assuming that its complex frequency response remains the same in all three recording channels: E_r, H_{WE}, and H_{SN}. The receiver gain as the function of frequency is shown in Figure 9.

Here the abscissa shows the signal frequency in hertz on the logarithmic scale. The gain (amplitude characteristic) of the receiver is shown by a smooth line plotted along the left ordinate in decibel. The phase characteristic of the receiver is measured in radians, and it is plotted by a dash-dotted line along the right ordinate.

The band-pass width of ELF receiver is formed by the Butterworth high-pass filter of fourth order with the cutoff frequency of 4 Hz and by the Butterworth low-pass filter of sixth order with the 40-Hz cutoff frequency. The notch filter at 50 Hz provides the attenuation of the signals from the power supply network by 240 dB. Such a receiver allows us to significantly reduce the industrial noise and to decrease the interference from the local weather conditions due to the optimal choice of cutoff frequencies (Nickolaenko & Hayakawa, 2002, 2014).

The most straightforward and expected modification of the pulse shape at the output of the Schumann resonance receiver will be its widening, as the spectrum of the input pulse occupies the wider bandwidth than that of the receiver. In addition, as was shown by Yatsevich et al. (2014), the influence of a typical receiver leads to a delay of the output pulsed signal relative to the input pulse and to modification output pulse waveform. In particular, the ratio alters of amplitudes of the positive and the negative half waves at the pulse onset, which might lead in some cases to incorrect attribution of the lightning stroke polarity when an actually positive discharge is classified as a negative one.

To obtain the pulsed waveforms at the output of the Schumann resonance receiver, we multiplied the model spectra of $E_r(f)$, $H_{WE}(f)$, and $H_{SN}(f)$ field components by the frequency dependent complex gains of the receiver $G(f)$ and afterward performed the Fourier transform of these products. The obtained temporal realizations are depicted by plots of Figures 10 and 11.

10.1029/2018JD028951

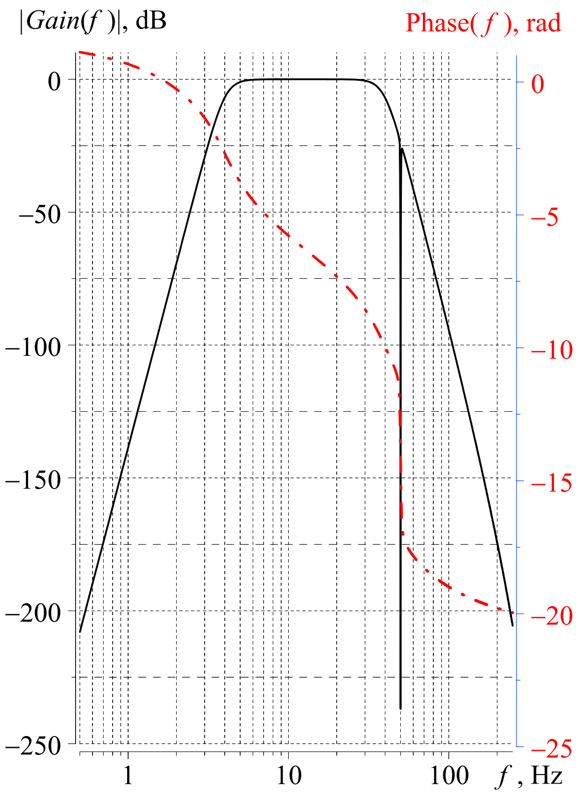

Figure 9. Amplitude and phase characteristics of an idealistic Schumann resonance receiver.

Figure 10 demonstrates the pulsed waveforms and relevant hodographs of two mutually orthogonal magnetic field components for propagation paths corresponding to $t_U = 4$ and $t_U = 8$ hr.

The left panel (Figure 10a) demonstrates the results corresponding to $t_U = 4$ hr, and the right one is relevant to $t_U = 8$ hr. As before, the major plots show the temporal variations of the horizontal magnetic fields. Data are presented in the same way as in Figure 7: the regular field component H_{WE} is plotted on the left ordinate, and the H_{SN} field is shown of the right ordinate.

The field hodographs or Lissajous figures of the corresponding pulses are shown at the upper left corner of each panel. Obviously, the pulses became substantially wider at the output of the receiver, and their onset is shifted in time. The Lissajous figures also have changed noticeably in comparison with Figure 7. Now, the outline of the curves is significantly dependent on the location of propagation path relative to the terminator line. Simultaneously, establishing the direction toward the field source remains problematical as the field hodograph indicates.

Schumann resonance signals at the output of the receiver might be used from obtaining the temporal variations of the orthogonal horizontal components of the Umov-Poynting vector, as well as the hodographs of this vector. The corresponding results are collected in Figure 11 in the same form as it was done in Figure 8. One may see that the pulse of the power flow was appreciably expanded at the output of the ELF receiver. It is worth noting that the major $P_{NS}(t)$ pulse, which is directed from the north to the south in the main energy flow, consists of two distinct positive subpulses. One can also resolve a pair of pulses in the original power flux of Figure 8, but there the first short smaller pulse practically merges with the higher second one.

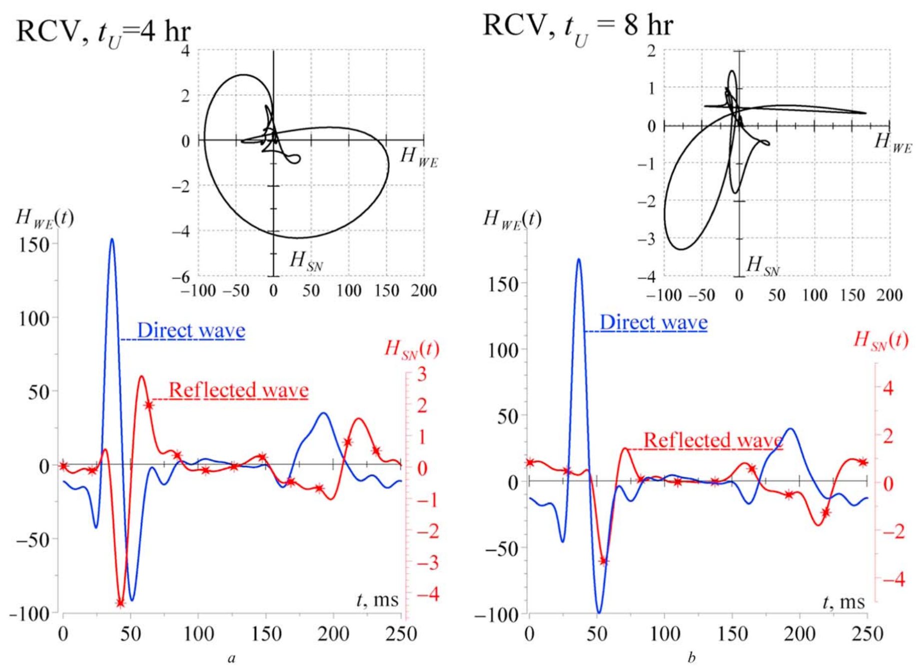

Figure 10. Magnetic fields and their hodographs at the output of a typical extremely low frequency receiver. (a) The propagation path location corresponds to $t_U = 4$ hr; (b) corresponds to $t_U = 8$ hr.

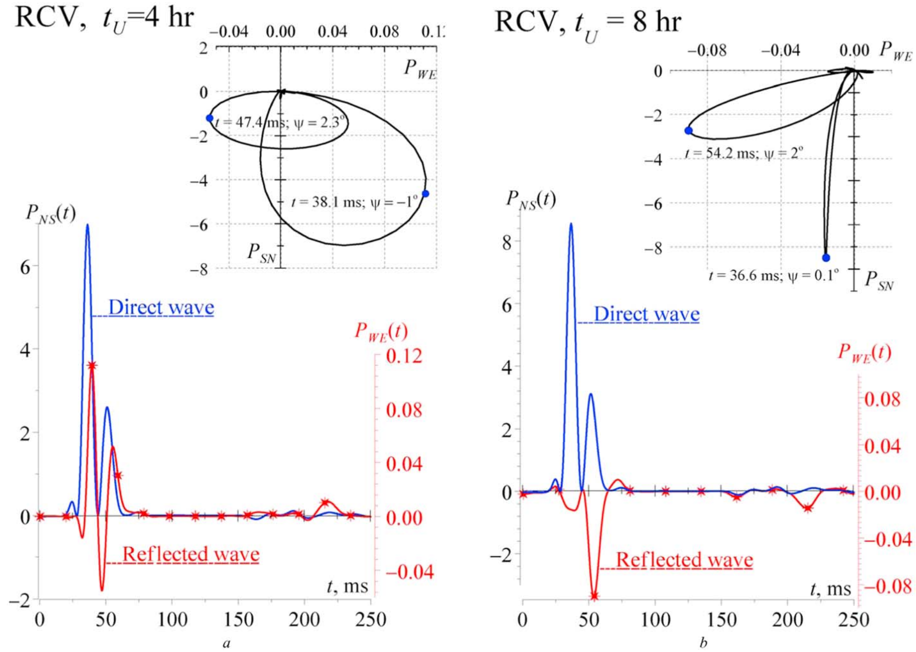

Figure 11. Waveforms and hodographs of the Umov-Poynting vector at the output of a typical extremely low frequency receiver of 4–40-Hz bandwidth. (a) Position of propagation path corresponds to 4 hr UT; (b) location of the path corresponds to 8 hr UT.

Outline of temporal variations in the power flux associated with the wave reflections from the day-night nonuniformity also greatly changed at the output of the receiver with a finite bandwidth. Waveform significantly depends on the position of propagation path relative to the terminator line, especially in the P_{NS} component. These peculiarities are able to significantly change the results of source bearing measurements.

Now, the Umov-Poynting vector deviates from the true north-south direction for t_U = 4 hr having the maximum deviation to the east observed on 38.1 ms after the lightning stroke initiation marked in the hodograph plot by blue circle. The relevant deviation of the source bearing is −1° (from north to west). This is followed by excursion of the Umov-Poynting vector tip to the west with the maximum on 47.4 ms. The relevant source bearing reaches 2.3° directed toward the east. We remind that times of maximum excursions were 18.1 and 20.5 ms correspondingly in the absence of ELF receiver. When t_U = 8 hr, the Umov-Poynting vector almost does not deviate from the true north-south direction. The maximum departures are observed on 36.6 and 54.2 ms after the initiation of lightning discharge. The relevant angular errors in the source bearing are 0.1° and 2.3°. These excursions were observed on 18.6 and 20.5 ms without ELF receiver. We observe that a receiver noticeably alters the time and the outline of hodographs, but the angular deviations from the regular direction of the power flux (the meridian plane) remain rather small, ~2° utmost.

Thus, impact of the ionosphere day-night nonuniformity on the power flux of Q-bursts at the output of a typical receiver turns out to remain very small. The detection of the terminator impact on the source bearing with deviations of 3° (~0.05 rad.) becomes possible when the ELF transient amplitude exceeds the root-mean-square value of the continuous background signal formed by radiation of global thunderstorms by the factor of 20 or higher. We must admit that model computations predict the impact of the day-night nonuniformity, which does not exceed the natural fluctuations due to continuous background radiation from the planetary thunderstorm activity. Thus, a detection of the terminator effect in the source bearing might be possible only for exceptionally rare powerful lightning strokes.

7. Conclusions

Modeling performed and the data analysis allow us to formulate the following conclusions:

1. Deviations in the source bearing depend on the frequency, on the propagation path length, and its position relative to the day-night interface. Impact of the terminator is absent when the center of propagation

path is coincident with the center of the night or the day hemisphere. The effect of day-night nonuniformity increases when the path comes closer to the solar terminator line. The source bearing deviations can reach several degrees at some frequencies when the propagation path is located near the day-night interface. Such deviations become comparable with the source azimuth fluctuations conditioned by permanent continuous background noise in the Schumann resonance band originating from radiation of planetary lightning activity.
2. The source bearing varies with frequency thus reflecting the influence of global electromagnetic (Schumann) resonance.
3. Deviation of the source bearing arises due to reflections of radio waves from the day-night nonuniformity, which produce a “longitudinal” component of horizontal magnetic field oriented along the observer-source arc. Temporal variations of magnetic field components oriented along and across the propagation path acquire complicated shape. In the case of a monochromatic radio signal, a weak elliptical polarization is observed having the altering sign (the rotation direction of the total magnetic field vector) when the propagation path moves from one side of the day-night interface to the other.
4. For the pulsed signals (ELF transients or Q-bursts), the waveforms in orthogonal field components become rather complicated. The total magnetic field hodograph outlines intricate closed curves, and this hampers finding of the wave arrival angle.
5. Impact of the day-night nonuniformity on the observed source bearing is rather small. In addition, the waveforms depend substantially on the frequency response of ELF receiver. The results obtained at different sides of the day-night interface deviate significantly from each other. However, the maximum instantaneous deviations in the source bearing do not exceed several degrees. To detect such small deviations in the presence of continuous background radio noise from the global thunderstorms, one will have to select the rare pulses of amplitude exceeding the root-mean-square amplitude of Schumann resonance background by a factor of 20 or higher.

Data Statement

All the data used in our paper are listed in the references.

References

Belyaev, G. G., Schekotov, A. Y., Shvets, A. V., & Nickolaenko, A. P. (1999). Schumann resonance observed with the Poynting vector spectra. *Journal of Atmospheric and Solar - Terrestrial Physics*, *61*(10), 751–763. https://doi.org/10.1016/S1364-6826(99)00027-9

Bliokh, P. V., Nickolaenko, A. P., & Filippov, Y. F. (1980). In D. Llanwyn Jones (Ed.), *Schumann resonances in the Earth-ionosphere cavity* (p. 168). London, New York: Peter Peregrinus ltd.

Galuk, Y. P., Nickolaenko, A. P., & Hayakawa, M. (2018). Amplitude variations of ELF radio waves in the Earth-ionosphere cavity with the day-night non-uniformity. *Journal of Atmospheric and Solar - Terrestrial Physics*, *169*, 23–36. https://doi.org/10.1016/j.jastp.2018.01.001

Galuk, Y. P., Nickolaenko, A. P., & Hayakawa, M. (2015). Comparison of exact and approximate solutions of the Schumann resonance problem for the knee conductivity profile. *Telecommunications and Radio Engineering*, *74*(15), 1377–1390. https://doi.org/10.1615/TelecomRadEng.v74.i15.60

Hynninen, E. M., & Galuk, Y. P. (1972). Field of vertical electric dipole over the spherical Earth with non-uniform along height ionosphere. In *Problems of diffraction and radio wave propagation* (Vol. 11, pp. 90–120). Leningrad: Leningrad State University Press. (in Russian)

Kirillov, V. V. (1996). Two-dimentional theory of ELF electromagnetic wave propagation in the Earth–ionosphere waveguide channel. *Radiophysics and Quantum Electronics*, *39*, 9, 737–743.

Kirillov, V. V. (1998). Parameters of the two-dimensional telegraph equation at ELF. *Radiotechnology Electronics (in Russian)*, *43*(7), 779.

Kirillov, V. V., & Kopeykin, V. N. (2002). Solving a two-dimensional telegraph equation with anisotropic parameters. *Radiophysics and Quantum Electronics*, *45*(12), 929–941. https://doi.org/10.1023/A:1023525331531

Kirillov, V. V., & Kopeykin, V. N. (2003). Formation of a resonance structure of the local inductance of the ionosphere at frequencies 0.1–10 Hz. *Radiophysics and Quantum Electronics*, *46*(1), 1–12. https://doi.org/10.1023/A:1023652610575

Kirillov, V. V., Kopeykin, V. V., & Mushtak, V. K. (1997). Electromagnetic waves of ELF band in the Earth–ionosphere waveguide. *Geomagnetism and Aeronomy*, *37*(3), 114–120.

Kudintseva, I. G., Nickolaenko, A. P., Rycroft, M. J., & Odzimek, A. (2016). AC and DC global electric circuit properties and the height profile of atmospheric conductivity. *Annals of Geophysics*, *59*(5), 15. https://doi.org/10.4401/ag-6870

Kulak, A., Zieba, S., Micek, S., & Nieckarz, Z. (2003). Solar variations in extremely low frequency propagation parameters: 1. A two-dimensional telegraph equation (TDTE) model of ELF propagation and fundamental parameters of Schumann resonances. *Journal of Geophysical Research*, *108*(A7), 1270. https://doi.org/10.1029/2002JA009304

Madden, T., & Thompson, W. (1965). Low frequency electromagnetic oscillations of the Earth–ionosphere cavity. *Reviews of Geophysics*, *3*(2), 211–254. https://doi.org/10.1029/RG003i002p00211

Mlynarczyk, J., Kulak, A., & Salvador, J. (2017). The accuracy of radio direction finding in the extremely low frequency range. *Radio Science*, *52*, 1245–1252. https://doi.org/10.1002/2017RS006370

Nickolaenko, A., & Hayakawa, M. (2002). *Resonances in the Earth-ionosphere cavity* (p. 380). Dordrecht: Kluwer Academic Publ., Dordrecht-Boston-London.

Nickolaenko, A., & Hayakawa, M. (2014). *Schumann resonance for Tyros (Essentials of global electromagnetic resonance in the Earth–ionosphere cavity), Series XI, Springer Geophysics*, (). Tokyo: Springer. https://doi.org/10.1007/978-4-431-54358-9

Nickolaenko, A. P., Galuk, Y. P., & Hayakawa, M. (2017). Extremely low frequency (ELF) wave propagation: Vertical profile of atmospheric conductivity matching with Schumann resonance data. In A. Reimer (Ed.), Chapter 6*Horizons in world physics* (Vol. 288, pp. 105–128). New York: NOVA Sci. Publishers. ISBN: 978–1–63485-882-3, ISBN: 978–1–63485-905-9 (eBook)
Nickolaenko, A. P., Shvets, A. V., & Hayakawa, M. (2016a). Extremely low frequency (ELF) radio wave propagation: A review. *International Journal of Electronics and Applied Research (IJEAR)*, *3*(2), 81. Published online (http://eses.co.in/online_journal.html) ISSN 2395 0064
Nickolaenko, A. P., Shvets, A. V., & Hayakawa, M. (2016b). Propagation at Extremely Low-Frequency Radio Waves. In J. Webster (Ed.), *Wiley Encyclopedia of Electrical and Electronics Engineering* (pp. 1–20). Hoboken, USA: John Wiley. https://doi.org/ 10.1002/047134608X.W1257.pub2
Pechony, O. (2007). Modeling and simulations of Schumann resonance parameters observed at the Mitzpe Ramon field station, Ph. D. Thesis, Tel-Aviv, − 92 pp.
Pechony, O., & Price, C. (2004). Schumann resonance parameters calculated with a partially uniform knee model on Earth, Venus, Mars, and Titan. *Radio Science*, *39*, RS5007. https://doi.org/10.1029/2004RS003056
Samarskyj, A. A. (2001). *The theory of difference schemes*. NY: Marcel Dekker Inc.
Yatsevich, E. I., Shvets, A. V., & Nickolaenko, A. P. (2014). Impact of ELF receiver on characteristics of ELF transients. *Radiophysics and Quantum Electronics*, *57*(3), 176–186.